# Objective Analysis of Hyperreflective Outer Retinal Bands Imaged by Optical Coherence Tomography in Patients With Stargardt Disease

Jason C. Park,[1] Frederick T. Collison,[2] Gerald A. Fishman,[1,2] Rando Allikmets,[3,4] Jana Zernant,[3] Michelle Liu,[1] and J. Jason McAnany[1,5,6]

[1]Department of Ophthalmology and Visual Sciences, University of Illinois at Chicago, Chicago, Illinois, United States
[2]The Pangere Center for Hereditary Retinal Diseases, The Chicago Lighthouse for People Who Are Blind or Visually Impaired, Chicago, Illinois, United States
[3]Department of Ophthalmology, Columbia University, New York, New York, United States
[4]Department of Pathology and Cell Biology, Columbia University, New York, New York, United States
[5]Department of Psychology, University of Illinois at Chicago, Chicago, Illinois, United States
[6]Department of Bioengineering, University of Illinois at Chicago, Chicago, Illinois, United States

Correspondence: J. Jason McAnany, University of Illinois at Chicago, Department of Ophthalmology and Visual Sciences, 1855 W Taylor Street, Chicago, IL 60612, USA; jmcana1@uic.edu.

Submitted: March 25, 2015
Accepted: June 14, 2015

Citation: Park JC, Collison FT, Fishman GA, et al. Objective analysis of hyperreflective outer retinal bands imaged by optical coherence tomography in patients with Stargardt disease. *Invest Ophthalmol Vis Sci*. 2015;56:4662–4667. DOI:10.1167/iovs.15-16955

**Purpose.** To develop and apply an objective algorithm for analyzing outer retinal layers imaged by spectral-domain optical coherence tomography (SD-OCT) in patients with Stargardt disease (STGD1).

**Methods.** Horizontal macular B-scans were acquired from 20 visually normal controls and 20 genetically confirmed stage 1 STGD1 patients. The number of outer retinal bands was quantified using a semiautomated algorithm that detected bands using the second derivative of longitudinal reflectivity profiles. The present analysis focused on the three outermost bands, currently associated with the ellipsoid zone (EZ), cone outer segment interdigitation zone (IZ), and retinal pigment epithelium (RPE) complex.

**Results.** The RPE complex and EZ bands were detected throughout the B-scan in all controls. The RPE complex was detected throughout the B-scan in all patients, but was atrophic appearing in some locations. The EZ band was detected only outside the central lesion. Interdigitation zone band detection varied as a function of eccentricity for both groups, with detection for controls being highest in the para- and perifovea and lowest in the fovea and near periphery. In patients, the IZ band was generally not present in the fovea or para- or perifovea due to the central lesion. Outside of the lesion, the IZ band was detected in 26% of patients (mean detection across the near periphery), which was approximately half of the detection in controls.

**Conclusions.** An objective approach for quantifying the number of outer retinal OCT bands found reduced IZ detection in STGD1 patients. This occurred even outside the central lesion, demonstrating an inability to image the IZ, possibly due to enhanced RPE reflectivity or abnormal outer retinal structure.

Keywords: optical coherence tomography, image analysis, stargardt disease, cone interdigitation zone

Autosomal recessive Stargardt disease (STGD1; Online Mendelian Inheritance in Man [OMIM] 248200), which is due to mutations in the *ABCA4* gene,[1] affects 1 in 10,000 individuals and is the most common juvenile-onset hereditary macular dystrophy.[2] Dysfunctional *ABCA4* protein alters vitamin A aldehyde transport in the outer segments of photoreceptors, resulting in the formation of phototoxic bisretinoids of lipofuscin.[3] The lipofuscin is deposited in retinal pigment epithelium (RPE) cells during disc shedding and phagocytosis. Accumulation of lipofuscin is associated with many of the clinical features of STGD1, including fundus flecks, increased fundus autofluorescence, and atrophy of the outer retina.[4–10]

Several studies have evaluated retinal structure in patients with STGD1 using optical coherence tomography (OCT).[6,11–14] Although abnormal inner retinal structure has been reported in these patients,[13] the focus of previous studies has typically been on the four hyperreflective outer retinal bands that can be imaged by OCT. These four outermost retinal bands are currently associated with the (1) external limiting membrane (ELM), (2) photoreceptor ellipsoid zone (EZ) (but see Jonnal et al.[15]), (3) cone outer segment/RPE interdigitation zone (IZ), and (4) RPE–Bruch's membrane complex. In patients with STGD1, the ELM (band 1) can be abnormally thick[14]; the EZ (band 2) is typically missing at the site of the central lesion,[6,16] and the RPE complex (band 4) can be abnormally thin.[6] Although the characteristics of the IZ band (band 3) have not been reported in patients who have STGD1, previous work has shown that this band is absent in patients with cone-rod dystrophy (CRD),[17] which is a hereditary retinal degenerative

TABLE. Patient Characteristics

| Patient No. | Age, y | Sex | BCVA | No. of *ABCA4* Mutations | Mutation(s) |
|---|---|---|---|---|---|
| 1 | 13 | M | 20/70 | 2 | p.[(L541P; A1038V)](;)c.5714+5G>A |
| 2 | 15 | F | 20/60 | 2 | c.3050+5G>A(;)p.(G1961E) |
| 3 | 15 | F | 20/80 | 2 | p.[(R1129L(;)A1773V)] |
| 4 | 16 | F | $10/100^{-1}$ | Sister of patient 3 | |
| 5 | 20 | M | $20/160^{+2}$ | 2 | p.[(R1129C(;)R2077W)] |
| 6 | 20 | F | $20/160^{-1}$ | 2 | p.[(G1961E(;)R2040*)] |
| 7 | 21 | M | 20/40 | 2 | p.[(R219T(;)W439*(;)G863A)] |
| 8 | 23 | F | 10/100 | 2 | c.5461-10T>C(;)p.(G1961E) |
| 9 | 23 | F | $20/100^{-1}$ | 2 | c.302+1G>A(;)p.(R2107H) |
| 10 | 28 | F | $20/100^{-1}$ | 2 | c.5461-10T>C(;)p.(G1961E) |
| 11 | 30 | F | $20/25^{+2}$ | 1 | p.[(R2077W)];[?] |
| 12 | 31 | F | 20/200 | 2 | p.(G1961E);c.6479+1G>A |
| 13 | 31 | F | $20/125^{-1}$ | 1 | p.[(Q636*)];[?] |
| 14 | 33 | F | 20/200 | 2 | p.[(L541P;A1038V(;)I1684N)] |
| 15 | 41 | F | $20/25^{+1}$ | 2 | p.[(V989A)];[(V989A)] |
| 16 | 45 | F | 20/25 | 2 | p.[(I975M(;)K1978E)] |
| 17 | 45 | M | 20/200 | 2 | p.[(R1108C;Q876P)];[(Q876P)] |
| 18 | 47 | F | 20/200 | 2 | p.[(R1108C(;)G1961E)] |
| 19 | 48 | M | $20/25^{-3}$ | 2 | p.[(G1961E)];[(G1961E)] |
| 20 | 48 | M | 20/100 | 2 | p.[(G863A)];[(G863A)] |

BCVA, best-corrected visual acuity; "?" indicates that the second mutation was not identified.

* Denotes a stop codon.

disease that can also be caused by *ABCA4* mutations. Abnormalities in this band might be expected in patients with STGD1, given that RPE and photoreceptor cells are the primary sites of abnormality in STGD1 and there is genetic overlap between CRD and STGD1.

At present, the retinal source of the IZ band is uncertain. As reviewed elsewhere,[15] the band was identified by adaptive-optics OCT (AO-OCT),[18] and two likely origins of the IZ band have been proposed: (1) the tips of the cone outer segments (OS)[19,20]; (2) light that is scattered from a more distal source (e.g., the RPE) onto the tips of the cone OS, which act as waveguides. Additional work is needed to evaluate these two possible sources. Despite the uncertainty of its origin, we refer to this band as the interdigitation zone (IZ) in the present study, as recommended by the International Nomenclature for OCT (IN-OCT) committee.[21]

The purpose of the present study was to develop and apply an objective, semiautomated algorithm for analyzing the layers of the outer retina imaged by spectral-domain OCT (SD-OCT) in patients with STGD1. The present study focused on the three outermost retinal bands (RPE complex, IZ, and EZ) with a particular emphasis on the IZ, as little has been reported regarding this band in STGD1. Previous studies that have assessed the integrity of the IZ band in CRD,[17] choroideremia,[22] and acute zonal occult outer retinopathy[23] and in patients who have a macular hole[24] have used subjective approaches in which experienced graders measured the length of the IZ band using software provided by the OCT manufacturer or provided qualitative assessments of the OCT scans. The present study used a different approach: The number of hyperreflective outer retinal bands was quantified for each subject using a novel semiautomated algorithm that detected the number of hyperreflective bands based on longitudinal reflectivity profiles (LRPs) as follows: (1) Horizontal macular B-scans were acquired; (2) the B-scans were divided into 25 equally spaced columns and the A-scans within a column were averaged; (3) an LRP (i.e., OCT reflectivity along the averaged A-scan) was generated for each column; (4) the number of bands was quantified based on the second derivative of the LRP. This procedure was performed in genetically confirmed STGD1 patients and in visually normal control subjects.

## MATERIALS AND METHODS

### Subjects

Twenty patients with stage 1 STGD1 (6 males and 14 females) with a mean age (±SD) of 29.7 ± 12.2 years participated in this study. Stage 1 STGD1 is defined by fundus flecks confined to the macula, typically distributed in a ring around the fovea.[8] Patients with stage 1 STGD1 were selected because these patients generally have more stable fixation, compared to STGD1 patients with more advanced stages, and the clinical appearance of the retina is relatively normal outside of the central macular lesion and ring of flecks. The patients' age, sex, best-corrected visual acuity, number of identified *ABCA4* mutations, and the specific mutation(s) identified are summarized in the Table. Among the 20 patients, 17 were positive for at least two disease-causing variants of the *ABCA4* gene; 2 were positive for a variant on one allele, and 1 patient was untested but was the sibling of a patient with two identified *ABCA4* mutations. No patient had clinically significant ocular media opacities, a history of significant ocular comorbidities, or spherical refractive error greater than 6.0 diopters with the exception of patients 11 and 15, who had spherical equivalents of –6.50 and –7.25, respectively. Twenty control subjects (12 males and 8 females) with a mean age (±SD) of 33.9 ± 6.6 years also participated in this study. The mean ages of the controls and patients did not differ significantly ($t = 1.37$, $P = 0.18$). All control subjects had best-corrected visual acuity of 0 logMAR or better (equivalent to Snellen acuity of 20/20 or better), spherical refractive error less than 6.0 diopters, normal Pelli-Robson contrast sensitivity, and no history of visual abnormalities. The procedures adhered to the tenets of the Declaration of Helsinki and were approved by Institutional Review Boards. Informed consent was obtained from each subject before his/her participation.

### SD-OCT Imaging and Analysis

Optical coherence tomography images were obtained using an Optos spectral-domain OCT/scanning laser ophthalmoscope (SLO) instrument (Optos PLC, Dunfermline, UK). Optical coherence tomography data were obtained from the right eye of all subjects, with the exception of two patients from whom data from the left eye were obtained. For these two patients, the image quality of the right eye was poor, so data were obtained from the left eye and converted to right eye format for analysis. The signal quality reported by the instrument was the same (10/10) for all subjects.

Custom-written MATLAB software (MATLAB; The MathWorks, Natick, MA, USA) was used to quantify the number of hyperreflective outer retinal bands, illustrated in Figure 1, as follows:

1. B-scans (9.0 by 1.5 mm) were acquired along the horizontal meridian, centered on the fovea. The B-scans were divided into 25 columns that were each 305 μm in width (each column included 43 adjacent A-scans, spanning approximately 1° of visual angle). The vertical white lines in Figure 1A indicate the columns; the distances from the foveal center (degrees) are marked, with negative values indicating measurements from the

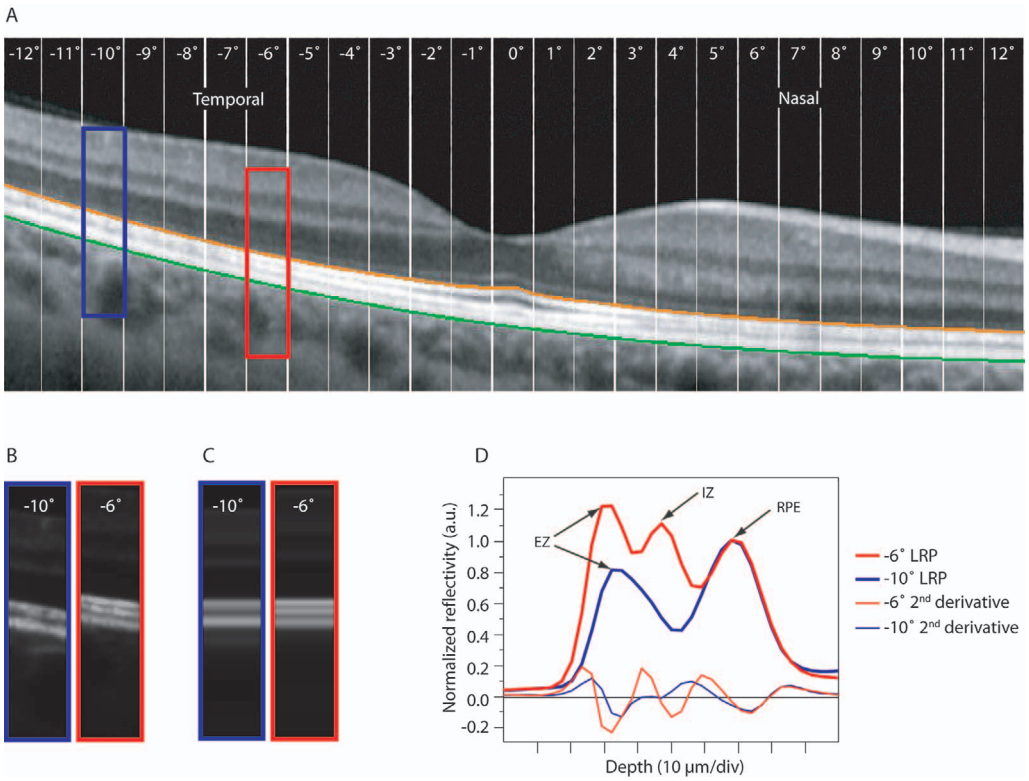


**Figure 1.** Illustration of the approach used by the semiautomated detection algorithm. (**A**) The B-scan from a control subject divided into 25 columns, each subtending 1° of visual angle (indicated by the numbers). Negative retinal eccentricities indicate measurements made from the temporal retina, whereas positive retinal eccentricities indicate measurements made from the nasal retina. The *orange* (EZ) and *green* (RPE) *lines* define the outer retina. (**B**) The linearized OCT reflectivity profiles obtained at −10° and −6°. (**C**) The averaged linearized OCT reflectivity profiles from these two columns. (**D**) The LRPs from columns −10 (*thick blue profile*) and −6 (*thick red profile*). The *thin red* and *blue profiles* at the *bottom* of the plot represent the second derivatives of the LRPs measured at −10° and −6°, respectively.

temporal retina and positive values indicating measurements from the nasal retina.

2. The EZ and RPE bands were identified, using a semiautomated approach,[25] to define a spatial region to be searched (Fig. 1A; orange and green lines).
3. The OCT B-scan reflectivity was linearized (anti-log) to allow small differences in hyperreflective regions to be better visualized, as discussed elsewhere.[20] Figure 1B shows an example of linear reflectivities from −10°, where two hyperreflective bands were visible, and from −6°, where three hyperreflective bands were visible.
4. Each of the 43 A-scans within a column was shifted vertically to align the A-scans at the interface between the RPE and Bruch's membrane, which corrected curvature and tilt of the scan. The shifted A-scans within each column were then averaged. Figure 1C shows an example of averaged linear reflectivities from −10° and from −6°. Averaging reduced image noise and permitted the number of bands to be better visualized.
5. Longitudinal reflectivity profiles were generated, which are plots of OCT reflectivity at each point in a column, as shown by the thick red and blue profiles in Figure 1D. The thick red profile (−6°) had three prominent peaks, corresponding to the EZ, IZ, and RPE complex bands. In comparison, only two peaks, corresponding to the EZ and RPE complex, were visible in the column from −10° (thick blue profile).
6. The second derivative of each LRP was computed and the number of zero crossings was determined to quantify the number of hyperreflective bands in each column (thin red and blue profiles shown in the lower portion of Fig. 1D). Of note, compared to the first derivative, the second derivative was better able to detect subtle changes in the LRP.

## Manual Grading

To evaluate the validity of the objective algorithm, the number of hyperreflective outer retinal bands visible in standard B-scans (e.g., Fig. 1A) was determined by four experienced graders (JCP, FTC, ML, JJM). The results of the four graders were averaged and compared to those provided by the automated algorithm. The four graders and the semiautomated algorithm had excellent agreement, such that the algorithm and at least three of the four graders were in agreement in 85% of the retinal locations analyzed; agreement between the graders and the algorithm is discussed further below.

## Results

The RPE and EZ bands were detected throughout the entire B-scan in all controls, as expected. A band of variable thickness that corresponds to the RPE complex was detected throughout the entire B-scan in all STGD1 patients, whereas a band that corresponds to the EZ was detected only outside of the central lesion. Figure 2 shows the percentage of patients for whom an EZ band was detected by semiautomated segmentation (step 1 above) for each of the 25 retinal locations sampled. In the central foveal and parafoveal areas (0° to ±3° columns), the EZ

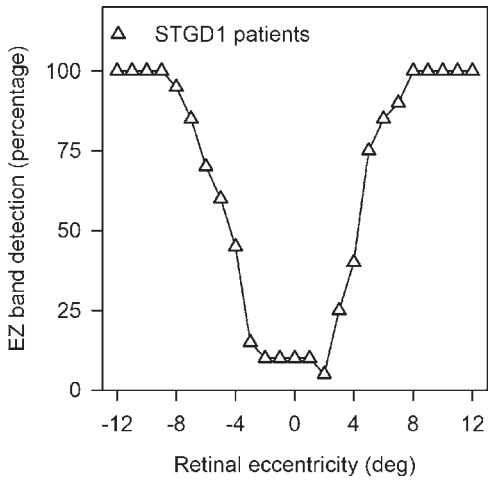


FIGURE 2. The percentage of STGD1 patients with a visible EZ band is shown for each of the 25 sampled retinal locations.

band was detected in only a small percentage of patients (average of 12% over this region) due to the central lesion. Two patients (11 and 16) had relatively well-preserved EZ at the foveal center (bull's-eye macular lesion), and these two patients had relatively good visual acuity. However, outside of the central lesion, the percentage of patients with a detectable EZ band increased sharply. For eccentricities greater than ±9°, the EZ band was visible for all STGD1 patients.

Figure 3A plots the percentage of control subjects who had a detectable IZ band for each of the 25 sampled retinal locations. Mean detection (±1 SD) by the graders is represented by the blue open circles, and detection by the algorithm is represented by the red filled circles. At the foveal center (column 0), the IZ was detected in 63% (manual) and 50% (algorithm) of the controls. The probability of detection increased as eccentricity from the fovea increased, peaking in the parafovea (approximately ±3° [±1365 μm] from the foveal center), with a mean detection by the algorithm at ±3° of 97.5%. For locations greater than ±5° from the foveal center, the probability of IZ band detection decreased, with approximately 90% to 45% of the controls having a detectable IZ band, depending on location (±5° to ±12°).

Figure 3B shows the percentage of STDG1 patients who had a detectable IZ band for each of the 25 sampled retinal locations. The semiautomated algorithm (red filled triangles) and manual analysis (blue open triangles) showed good agreement, but there was some discrepancy in the temporal retina, with less frequent detection by the graders. There was also some disagreement among the four graders over this region, as denoted by the error bars (±1 SD). In the nasal perifoveal region and beyond (>5°, >1667 μm), the percentage of patients for whom the IZ band was detected was low: 5% to 21% (graders) and 5% to 30% (algorithm), depending on location. Across this region, percent detection tended to increase as eccentricity increased. A similar pattern was observed in the temporal retina, where percent detection increased as eccentricity increased from –6° to –12° (15%–35% depending on location, algorithm determined; 4% to 30% depending on location, grader determined).

Figure 3C replots the semiautomated band detection results for the controls (circles) and STGD1 patients (triangles) together to facilitate direct comparisons. Interdigitation zone band detection was most different between the two groups in the parafovea (±2° to ±4° from the foveal center), where mean detection over this region was 89% for the controls and only 3% for the STDG1 patients. The large difference in this region can be attributed to the central lesion, as the EZ band was disrupted in this region for most of the patients. All of the patients had an intact EZ band at eccentricities greater than ±9°, but the IZ band detection in these regions was still lower than normal. Specifically, IZ band detection in STGD1 patients at eccentricities greater than 9° was reduced compared to normal in the nasal retina, where the band was detected in approximately 55% to 70% of controls and 5% to 30% of the patients, depending on location. Interdigitation zone band detection in the STDG1 patients was also reduced in the temporal retina (–9° to –12°), but the reductions were somewhat less compared to the nasal retina: 45% to 85% for the controls and 30% to 40% for the patients, depending on location.

The data of Figure 3C raise the question whether the reflectivities of the outer retinal bands within and outside of the central lesion are similar in STGD1 patients, and how these reflectivities compare to normal. To address this question, the LRPs measured in STGD1 patients at the site of the central lesion and outside of the central lesion and in control subjects were compared (Fig. 4). The dashed red line in Figure 4 shows the LRP averaged over all patients at the site of the central lesion (i.e., locations in which the EZ was absent). The solid red line represents the LRP averaged over all patients outside of the central lesion (i.e., locations in which the EZ was present and the IZ was absent). The dashed blue line represents the control LRP averaged over all locations outside of the fovea for which the IZ band was not detected.

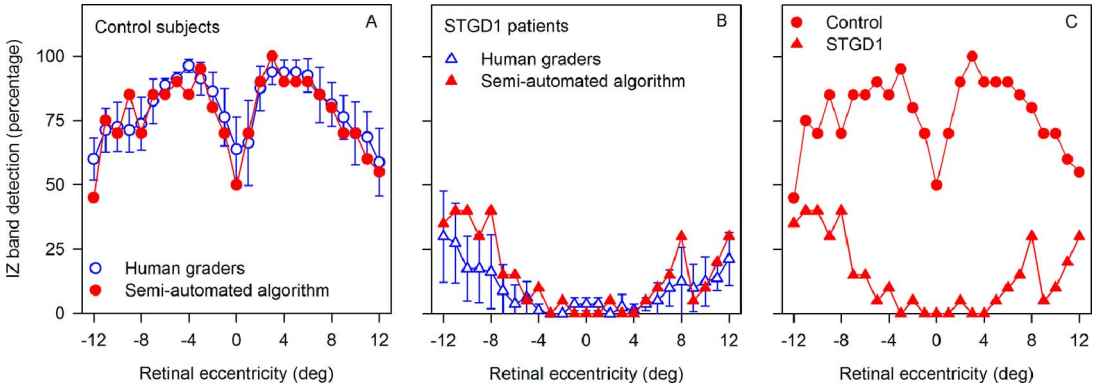


FIGURE 3. The percentage of IZ band detection for the control subjects (**A**) and STGD1 patients (**B**) is shown for each of the 25 sampled retinal locations. Detection by graders and the semiautomated algorithm is represented by the *open* and *filled symbols*, respectively. (**C**) Plot of the control and STGD1 semiautomated detection data together for comparison.

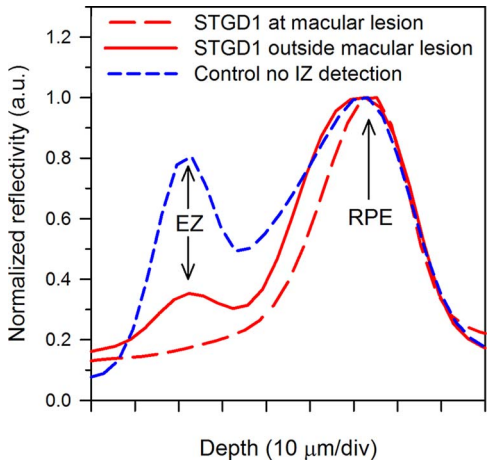


FIGURE 4. Reflectivity (arbitrary units; normalized to the RPE) is plotted as a function of retinal depth. The *dashed red line* represents the LRP averaged over all patients at the site of the central lesion (i.e., locations in which the EZ and IZ were absent). The *solid red line* represents the LRP averaged over all patients outside of the central lesion (i.e., locations in which the EZ was present and the IZ was absent). The *dashed blue line* represents the control LRP averaged over all locations outside of the fovea for which the IZ band was not detected.

Figure 4 shows that the LRP for patients measured outside of the central lesion at locations where the IZ was not detected is characterized by two hyperreflective regions that correspond to the EZ and RPE complex (solid red profile). In comparison, the LRP measured within the central lesion is characterized by a single hyperreflective region corresponding to the RPE complex (dashed red profile). Reflectivity of the RPE complex measured within the central lesion was narrower than the reflectivity measured outside of the central lesion, which is likely attributable to RPE atrophy at the site of the central lesion. The hyperreflective region corresponding to the RPE complex for the controls and the patients outside of the central lesion had similar widths (solid red and dashed blue profiles). Thus, the reflectivity profile of the RPE complex outside of the central lesion was similar to normal, but, not unexpectedly, different from the reflectivity profile within the central lesion. Furthermore, for the control subjects and STGD1 patients, the EZ reflectivity was less than the RPE complex reflectivity. Although this pattern was observed for both groups, the difference between EZ and RPE complex reflectivity was exaggerated in the patients compared to the controls.

## DISCUSSION

The present study developed and applied an objective, semiautomated algorithm for analyzing the layers of the outer retina imaged by SD-OCT. The algorithm was applied to SD-OCT scans from patients with STGD1 and visually normal controls to compare the number of hyperreflective bands in these two groups. The results showed that the RPE complex was present throughout the entire scan in all STGD1 patients, but was often atrophic appearing at the site of the central lesion. The EZ band was typically present only outside of the central lesion, as expected from previous work.[6,16] The current report also showed that the IZ band was absent at the site of the central lesion and, despite an intact EZ band, that the IZ band was less frequently detected in the near periphery. Specifically, the IZ band was detected across the near-peripheral retina (±9° to ±12° from the central fovea) in 45% to 85% of controls and 5% to 40% of the patients, depending on location.

The present study also provides a quantitative normative baseline to compare IZ band detection to patient populations. That is, previous work has described the IZ band as appearing separate from the RPE band outside of the fovea but merging with the RPE band in the central fovea in visually normal controls.[20] We confirm this finding quantitatively and extend it to show that the IZ band also often merges with the RPE band in the near periphery. There was, however, substantial variation in IZ band detection among the visually normal controls, with detection in some controls throughout the entire B-scan and large regions of missing IZ band detection in other controls. Thus, the present findings emphasize that the absence of IZ band detection with SD-OCT, even over relatively large regions, is not necessarily indicative of pathology.

A previous report of IZ visibility in patients with CRD showed a complete absence of the IZ band throughout the entire B-scan in all patients studied.[17] In comparison, only four of the 20 STGD1 patients in the present study had no detectable IZ band at any location examined. The absence of the IZ band in these four STDG1 patients suggests that its complete absence is not unique to patients with CRD. The large majority of our patients (16/20), however, had a detectable IZ band in at least some retinal locations. Differences in the degree of IZ band detection in stage 1 STGD1 and CRD may be expected, given that retinal structure and function of the peripheral retina tend to be less affected in stage 1 STGD1 patients compared to CRD patients.

As noted in the introduction, the retinal source of the IZ band is uncertain at present, but the tips of the cone OS are a likely candidate.[19] Despite uncertainty in the retinal origin of the band, there are at least two possible explanations for its reduced visibility in our STGD1 patients: (1) The anatomical structure from which the band is generated is absent (or disrupted), or (2) the anatomical structure from which the band is generated is present, but it cannot be resolved by standard SD-OCT. Inability to resolve the band could be due, for example, to increased reflectivity of the adjacent RPE complex (e.g., Fig. 4). Additional studies are needed to determine the source of the reduced IZ visibility in STGD1 patients.

The width of the hyperreflective band generated by the RPE–Bruch's membrane complex differed within and outside of the central lesion in our STGD1 patients. The narrower width of this band measured within the central lesion site, compared to locations outside of the lesion, can likely be attributed to RPE atrophy within the lesion. Interestingly, the width of the RPE–Bruch's membrane band measured in the STGD1 patients outside of the central lesion was highly similar to that measured in the normal control periphery (for locations at which the IZ band was not detected). Of note, in retinal locations where the IZ band was not detected, the RPE band typically had higher reflectivity than the EZ band (Figs. 1, 4), whereas in retinal locations where the IZ band was detectable, the EZ band typically had greater reflectivity (e.g., Fig. 1). Similar RPE and EZ reflectivities for locations in which the IZ is present and different reflectivities for locations in which the IZ is absent are also apparent in LRPs from a visually normal subject shown in a previous report.[20] In the present study, this was generally found for both the control subjects and the STGD1 patients, but the difference between EZ and RPE reflectivity was exaggerated in the patients compared to the controls. A similar pattern of reflectivity (i.e., greater RPE complex reflectivity than EZ reflectivity) was observed for the patients in the standard log-transformed scans, indicating that reduced EZ reflectivity is not an artifact of the image linearization. This decrease in EZ reflectivity may suggest

Investigative Ophthalmology & Visual Science

photoreceptor changes, which could contribute to the loss of IZ band detection in STGD1 patients.

In summary, an objective, semiautomated approach can be used successfully to quantify the number of hyperreflective outer retinal bands visible by OCT. There is variation among visually normal individuals in the extent to which the IZ band is detected, but the band was detected in nearly all visually normal individuals in the parafovea (approximately 3° nasal and temporal to the foveal center). The IZ band was less frequently detected in STGD1 patients compared to controls, even outside the central lesion, suggesting an inability to image the IZ band, possibly due to enhanced RPE reflectivity or to abnormalities in outer segment structure and/or RPE interdigitation.

## *Acknowledgments*

Supported by National Institutes of Health Research Grants EY019510 (JJM), EY001792 (UIC core grant), EY021163 (RA), EY019861 (RA), and EY019007 (Columbia University core grant); Pangere Family Foundation (GAF, FTC); Foundation Fighting Blindness (RA, JZ); and unrestricted departmental grants from Research to Prevent Blindness (UIC and Columbia University).

Disclosure: **J.C. Park**, None; **F.T. Collison**, None; **G.A. Fishman**, None; **R. Allikmets**, None; **J. Zernant**, None; **M. Liu**, None; **J.J. McAnany**, None

## *References*

1. Allikmets R, Singh N, Sun H, et al. A photoreceptor cell-specific ATP-binding transporter gene (ABCR) is mutated in recessive Stargardt macular dystrophy. *Nat Genet*. 1997;15:236–246.
2. Bither PP, Berns LA. Stargardt's disease: a review of the literature. *J Am Optom Assoc*. 1988;59:106–111.
3. Quazi F, Lenevich S, Molday RS. ABCA4 is an N-retinylidene-phosphatidylethanolamine and phosphatidylethanolamine importer. *Nat Commun*. 2012;3:925.
4. Armstrong JD, Meyer D, Xu S, Elfervig JL. Long-term follow-up of Stargardt's disease and fundus flavimaculatus. *Ophthalmology*. 1998;105:448–457, discussion 457–458.
5. Bonilha VL, Rayborn ME, Bell BA, Marino MJ, Fishman GA, Hollyfield JG. Retinal histopathology in eyes from a patient with Stargardt disease caused by compound heterozygous ABCA4 mutations [published online ahead of print September 29, 2014] *Ophthalmic Genet*. doi:10.3109/13816810.2014.958861.
6. Burke TR, Rhee DW, Smith RT, et al. Quantification of peripapillary sparing and macular involvement in Stargardt disease (STGD1). *Invest Ophthalmol Vis Sci*. 2011;52:8006–8015.
7. Cideciyan AV, Swider M, Aleman TS, et al. ABCA4-associated retinal degenerations spare structure and function of the human parapapillary retina. *Invest Ophthalmol Vis Sci*. 2005;46:4739–4746.
8. Fishman GA, Stone EM, Grover S, Derlacki DJ, Haines HL, Hockey RR. Variation of clinical expression in patients with Stargardt dystrophy and sequence variations in the ABCR gene. *Arch Ophthalmol*. 1999;117:504–510.
9. Lois N, Holder GE, Bunce C, Fitzke FW, Bird AC. Phenotypic subtypes of Stargardt macular dystrophy-fundus flavimaculatus. *Arch Ophthalmol*. 2001;119:359–369.
10. Rotenstreich Y, Fishman GA, Anderson RJ. Visual acuity loss and clinical observations in a large series of patients with Stargardt disease. *Ophthalmology*. 2003;110:1151–1158.
11. Huang WC, Cideciyan AV, Roman AJ, et al. Inner and outer retinal changes in retinal degenerations associated with ABCA4 mutations. *Invest Ophthalmol Vis Sci*. 2014;55:1810–1822.
12. Lazow MA, Hood DC, Ramachandran R, et al. Transition zones between healthy and diseased retina in choroideremia (CHM) and Stargardt disease (STGD) as compared to retinitis pigmentosa (RP). *Invest Ophthalmol Vis Sci*. 2011;52:9581–9590.
13. Genead MA, Fishman GA, Anastasakis A. Spectral-domain OCT peripapillary retinal nerve fibre layer thickness measurements in patients with Stargardt disease. *Br J Ophthalmol*. 2011;95:689–693.
14. Lee W, Noupuu K, Oll M, et al. The external limiting membrane in early-onset Stargardt disease. *Invest Ophthalmol Vis Sci*. 2014;55:6139–6149.
15. Jonnal RS, Kocaoglu OP, Zawadzki RJ, Lee SH, Werner JS, Miller DT. The cellular origins of the outer retinal bands in optical coherence tomography images. *Invest Ophthalmol Vis Sci*. 2014;55:7904–7918.
16. Ergun E, Hermann B, Wirtitsch M, et al. Assessment of central visual function in Stargardt's disease/fundus flavimaculatus with ultrahigh-resolution optical coherence tomography. *Invest Ophthalmol Vis Sci*. 2005;46:310–316.
17. Lima LH, Sallum JM, Spaide RF. Outer retina analysis by optical coherence tomography in cone-rod dystrophy patients. *Retina*. 2013;33:1877–1880.
18. Zawadzki RJ, Jones SM, Olivier SS, et al. Adaptive-optics optical coherence tomography for high-resolution and high-speed 3D retinal in vivo imaging. *Opt Express*. 2005;13:8532–8546.
19. Zhang Y, Cense B, Rha J, et al. High-speed volumetric imaging of cone photoreceptors with adaptive optics spectral-domain optical coherence tomography. *Opt Express*. 2006;14:4380–4394.
20. Spaide RF, Curcio CA. Anatomical correlates to the bands seen in the outer retina by optical coherence tomography: literature review and model. *Retina*. 2011;31:1609–1619.
21. Staurenghi G, Sadda S, Chakravarthy U, Spaide RF; IN•OCT Panel. Proposed lexicon for anatomic landmarks in normal posterior segment spectral-domain optical coherence tomography: the IN•OCT consensus. *Ophthalmology*. 2014;121:1572–1578.
22. Syed R, Sundquist SM, Ratnam K, et al. High-resolution images of retinal structure in patients with choroideremia. *Invest Ophthalmol Vis Sci*. 2013;54:950–961.
23. Matsui Y, Matsubara H, Ueno S, Ito Y, Terasaki H, Kondo M. Changes in outer retinal microstructures during six month period in eyes with acute zonal occult outer retinopathy-complex. *PLoS One*. 2014;9:e110592.
24. Itoh Y, Inoue M, Rii T, Ando Y, Hirakata A. Asymmetrical recovery of cone outer segment tips line and foveal displacement after successful macular hole surgery. *Invest Ophthalmol Vis Sci*. 2014;55:3003–3011.
25. Hood DC, Cho J, Raza AS, Dale EA, Wang M. Reliability of a computer-aided manual procedure for segmenting optical coherence tomography scans. *Optom Vis Sci*. 2011;88:113–123.

Investigative Ophthalmology & Visual Science